ALGORITHM THEORETICAL BASIS DOCUMENT (ATBD)
FOR THE
ADEOS/AMSR SEA ICE ALGORITHM

Josefino C. Comiso
Laboratory for Hydrospheric Processes
NASA Goddard Space Flight Center

1. Introduction

During the last century, the average global temperature has been increasing at the rate of 0.05K per decade (Jones, 1999). Because of feedback effects associated with the high albedo of ice and snow, such increases in temperature are expected to be amplified in polar regions (Budyko, 1966). Recent observations suggest that the Arctic environment may indeed be changing. Limited submarine sonar data indicate that the Arctic sea ice cover has been thinning by more than one meter in the last few decades (Rothrock et al., 1999; Wadhams and Davis, 2000, and Tucker et al., 2001) while sea ice extent in the same region has declined by about 5 to 6% in the last two decades (Bjorgo et al., 1997; Parkinson et al, 1999). Even more intriguing is the observation that the perennial sea ice cover is retreating at the much faster rate of 7-8% per decade (Johannessen et al., 1999; Comiso, 2001). The implication of the latter if the rate persists is that in a matter of a little more than a century, the perennial sea ice cover may disappear completely, causing profound changes in the characteristics, climate, and ecology of the Arctic system. To get this phenomena in proper perspective, more in depth studies of the changes in the global sea ice cover and associated changes in the environment are needed.

Sea ice covers a significant fraction of the global oceans (about 5 to 8%) and is one of the most seasonal parameter on the Earth's surface. Its high albedo, which ranges from about 80% (Grenfell, 1983) to 98% (Vowinckel and Orvig, 1970), compared to that of the open ocean (10% to 15%) minimizes heat absorbed by the surface and results in a sharp contrast in energy flux between ice free and ice covered oceans. This abrupt change in energy exchange can, under appropriate conditions, affect atmospheric circulation and give rise to violent weather systems known as polar lows (Carleton, 1985; Businger and Reed, 1989; Gloersen et al., 1989). Sea ice with its snow cover is also an effective insulator that limits the exchange of energy and momentum between the ocean and atmosphere. For example, in winter, the heat flux in an open lead exceeds by two orders of magnitude the heat flux through an adjacent thick ice cover (Badgley, 1966; Maykut, 1978). A large fraction of world's deep and bottom water is believed to be formed at polar latitudes (Stommel, 1962; Gordon, 1978; Killworth, 1983). Coastal polynyas near shelves around the Antarctic continent have been noted as ice factories and principal sources of bottom water (Zwally et al., 1985; Comiso and Gordon, 1998). The cold, dense water formed from sea ice growth in Arctic coastal polynyas helps maintain the Arctic Ocean halocline (Aagaard et al., 1981; Cavalieri and Martin, 1994). This dense water can also induce convection and deepen the mixed layer. Similar phenomenon is observed in the Odden, which is an ice tongue formation in Greenland Sea (Shuchman et al., 1996; Comiso et al., 2001) regarded as one of only four regions where open ocean convection occurs with the direct generation of deep water.

Because of its vast extent, large scale studies of the sea ice cover can be done most effectively through the use of satellite data. The later is available through various frequency channels from visible through infrared to microwave frequencies. Visible and infrared satellite data (e.g., AVHRR) have been used for mesoscale studies but the coverage of sea ice provided by the data is limited because of the persistence of cloud cover in polar regions. Detailed characterization of sea ice under all weather conditions has recently been provided by synthetic aperture radar (SAR) data (e.g., ERS-1, JERS-1, and Radarsat) but only a small fraction of the entire ice cover can be monitored at a time because of operational and data acquisition constraints and a narrow swath width (100 km to 500 km) that limits spatial and temporal resolution. These data sets have nonetheless been useful for regional studies and provide information that have been used to improve the interpretation of other satellite data.

The most comprehensive and consistent source of global sea ice data has been satellite passive microwave sensors (Zwally et al., 1983; Parkinson et al., 1987; Gloersen et al., 1992). Microwave sensors, not limited by weather conditions or light levels, are particularly well suited for monitoring sea ice, because of the strong

contrast in thermal microwave emission between areas of ice-free ocean and ice-covered waters. The first passive microwave sensor used extensively for studying the global distribution of sea ice was the Electrically Scanning Microwave Radiometer (ESMR) on board the NASA Nimbus 5 satellite (Gloersen et al., 1974; Zwally et al., 1983). The single channel ESMR, operating at 19.35 GHz, provided daily coverage of the polar regions and allowed for the first time synoptic observations of sea ice concentration needed for undertaking a detailed study of global sea ice variability. The ESMR sea ice algorithm was based on a linear relationship between the radiometric brightness temperatures of ice-free water and consolidated sea ice. Temperature variability effects were reduced using climatological data. At the ESMR frequency the contrast between ice and water is ~100 K. Although the estimated accuracy was only 15% (Comiso and Zwally, 1982), these data were used successfully to document sea ice changes in both hemispheres (Zwally et al.,1983; Parkinson et al., 1987).

The Scanning Multichannel Microwave Radiometer (SMMR) was launched on the SeaSat and Nimbus-7 research satellites in July 1978 and October 1978, respectively (Gloersen and Barath, 1977). With its multichannel capability, SMMR provided more information about the ice cover than ESMR. Multichannel SMMR algorithms extended the calculation of ice concentration to include the discrimination of two ice types, first-year and multiyear in the Arctic (Svendsen et al., 1983; Cavalieri et al., 1984; Swift et al., 1985) and sea ice temperature (Gloersen et al., 1992). Errors in the retrieval of multiyear ice concentration are, however, reported to be large (Kwok et al., 1996) because of the large variability in the emissivity of multiyear ice. A multichannel SMMR algorithm to obtain sea ice concentration only was also developed (Comiso and Sullivan, 1986; Comiso, 1986). The various algorithms take advantage of two or more channels to reduce errors associated with physical temperature variability, emissivity anomalies, and weather effects. In 1987, the first in a new series of passive microwave radiometers was launched as part of the Defense Meteorological Satellite Program (DMSP). This sensor, called the Special Sensor Microwave/Imager (SSM/I), operates at frequencies ranging from 19.4 GHz to 85.5 GHz. The SSM/I measures both horizontally and vertically polarized components at all frequencies except at 22.2 GHz for which only a vertically polarized component is obtained.

The advent of the Advanced Microwave Scanning Radiometer (AMSR) sensor, will mark a significant improvement in the capability for monitoring the sea ice cover. The new sensor will be basically a combination of both SMMR and SSM/I systems but with much better resolution. This means improvements in the ability to remove ambiguities in sea ice concentration through the use of the 6 and 10 GHz channels which have much better contrast in the signature of sea ice and open water than SSM/I channels. These channels also allow for the determination of ice temperature, which is an important polar parameter, and can be used to minimize uncertainties in the derived ice parameters that are associated with the spatial variability of ice temperatures. The high resolution data provided by the 85 GHz will also be useful in discriminating different surface types that may be associated with different emissivities.

2. Scientific Objectives

The specific objectives of this document are (a) to provide the theoretical basis of the algorithm that will be used to generate sea ice data sets from AMSR brightness temperatures; (b) to assess the accuracy of these products; and (c) to evaluate the range of applicability and the limitations of the derived data. Although passive microwave satellite data have been around for a while, AMSR will be a new high performing instrument that requires algorithms designed to take advantage of its added capabilities. AMSR data are expected to provide the baseline for new polar climate data sets and the means to evaluate the quality and consistency of historical satellite data. High quality and consistently derived sea ice parameters are needed to ensure that the time series data are suitable for climate change research (e.g., trend and mass balance studies).

Accurate and consistent data on sea ice cover are needed to fulfill some of the scientific goals of NASDA's ADEOS-II project. Among the objectives is to acquire data sets needed for climate change studies and meteorology research. More specifically for the polar regions is to study processes associated with sea ice, to improve and verify global circulation models (GCM), and to gain insights into the changing global climate as reflected in the polar regions. For process studies, it is important to detect and quantify the small but physically significant changes in the physical characteristics of the ice cover, especially in polynya and divergence areas and in the marginal ice zones. Accurate quantification of these polynyas and divergence areas are important in that they are the primary source of global bottom water (Gordon and Comiso, 1988; Martin et al., 1992). There should also be a good match of the sea ice cover as observed by satellites with those derived from GCMs. This

will ensure that the physical and mathematical formulation of these models as well as the assumptions made are based on solid foundations. Furthermore, studies of the changing ice cover and its future requires high standards in the quality and accuracy of retrieved satellite data (Bjorgo et al., 1997; Cavalieri et al., 1999; Comiso and Steffen, 2001). A fully validated algorithm for generating such a data set will go a long way towards fulfilling this goal.

3. AMSR Instrument Characteristics

The AMSR is a fourteen channel, eight-frequency total power passive microwave radiometer system that will be launched aboard the ADEOS-II satellite in 2002. It measures vertically and horizontally polarized radiances at 6.925, 10.65, 18.7, 23.8, 36.5, 50.3, 52.8, and 89.0 GHz. A second instrument, called AMSR-E, is a slightly modified version which will be launched on board EOS-Aqua satellite also in 2000. The ADEOS-II is a morning satellite while the EOS-Aqua is an afternoon satellite. Data from the two systems thus complement each other and will all be acquired and processed by NASDA's Earth Observation Center. AMSR consists of an offset parabolic reflector 2 m in diameter, fed by an array of seven feedhorns. The AMSR rotates continuously at 40 rpm about an axis parallel to the local spacecraft vertical. At an altitude of 802.9 km, it measures the upwelling scene brightness temperatures over an angular sector of + 61^o about the sub-satellite track, resulting in a swath width of 1600 km. During a period of 1.5 seconds the spacecraft sub-satellite point travels 10 km. Even though the instantaneous field-of-view (IFOV) for each channel is different, active scene measurements are recorded at equal intervals of 10 km (5 km for the 89 GHz channels) along the scan. The half-cone angle at which the reflector is fixed is 47.4^o which results in an Earth incidence angle of 55.0^o. Table 1 lists the pertinent performance characteristics

The radiometer calibration error, exclusive of antenna pattern correction effects, is composed of three major contributors: warm load reference error, cold load reference error, radiometer electronics nonlinearities and errors. An estimate of the warm load reference error is ~0.5 K, based on the RSS of the various components. The error in the cold reference measurement is mainly produced by the error in coupling between the cold sky reflector and the feedhorn. This is estimated to be ~0.5 K. The radiometer electronics nonlinearity results in an error that can be estimated during the thermal vacuum calibration testing (on SSM/I this error is ~0.4 K). A source of error in the receiver electronics is the gain drift resulting from temperature variations over one orbit. This error depends on the design of the receiver and overall design of the sensor. The gain drift can be as much as ~0.24 K for a temperature variation of less than 10 K over one orbit. Accounting for all errors, the total sensor bias error is 0.66 K at 100 K increasing with temperature to 0.68 K at 250 K.

Table 1. ADEOS AMSR SENSOR PERFORMANCE CHARACTERISTICS

CHARACTERISTICS	CENTER FREQUENCIES (GHz)							
	6.9	10.7	18.7	23.8	36.5	89.0	50.3	52.8
BANDWIDTH (MHz)	350	100	200	400	1000	3000	200	400
SENSITIVITY (K)	0.3	0.6	0.6	0.6	0.6	1.1		
IFOV (km x km)	76x44	49x28	28x16	31x18	14x8	6x4	12x8	12x8
SAMPLING RATE (km x km)	10x10	10x10	10x10	10x10	10x10	5x5		
INTEGRATION TIME (ms)	2.6	2.6	2.6	2.6	2.6	1.3		
BEAM EFFICIENCY (%)	95.3	95.0	96.3	96.4	95.3	96.0		
BEAMWIDTH (degrees)	2.2	1.4	0.8	0.9	0.4	0.18		

4. Standard and Research Products

The standard product for sea ice is sea ice concentration which is deemed essential to meet the overall scientific objectives of the ADEOS program. Ice temperature is also derived by the same algorithm and will be generated as a research product (Table 2). These products will be mapped to a standard polar grid currently used for the SSM/I (NSIDC, 1992). The grid resolutions for the AMSR brightness temperatures and sea ice concentrations were selected to take advantage of the full spatial resolution of the AMSR, while still providing continuity with

similar data from SMMR and SSM/I. Accuracies of the derived sea ice data will be determined with the aid of a comprehensive validation program described in section 5. In addition to the sea ice parameters, gridded brightness temperatures will also be provided at grid resolutions commensurate with the Level 2A spatially-averaged data (Table 2). Note that the 6.9 and 10.7 GHz data are gridded at a finer resolution than actual resolutions of about 58 and 37 km, respectively. The reason is to be able to use these channels in combination with higher frequency channels without losing too much on the resolution in the latter which are the primary channels for the algorithm. Further justification for using this gridding procedure will be presented later. It should be pointed out the sampling rate is 10x10 km for the 6.9GHz to 36.5 GHz channels and is 5x5 km for the 89 GHz channels. Also, observations at 6.9 and 10.7 GHz are produced at a spatial interval of approximately 20-km and at the sensor sampling rate for the other frequencies. Level 2A brightness temperature data will be convolved using the Backus-Gilbert method to provide the spatial averaging that is especially useful in the gridding the 6.9 and 10.7 GHz data at a finer resolution than actual resolution.

Table 2. AMSR Level 3 Tb and Sea Ice Data Sets

PARAMETER	APPROX. RESOL.	GRID RESOL. SIZE	TEMPORAL FOOTPRINT
6.9	58 km	25.0 km	
10.7	37 km	25.0 km	Daily Ascend., Decend., & Combined
18.7	21 km	25.0, 12.5 km	Daily Ascend., Decend., & Combined
23.8	21 km	25.0, 12.5 km	Daily Ascend., Decend., & Combined
36.5	11 km	25.0, 12.5 km	Daily Ascend., Decend., & Combined
89.0	5 km	25.0, 12.5, 6.25 km	Daily Ascend., Decend., & Combined
Sea Ice Conc.		25.0, 12.5 km	Daily Ascend., Decend., & Combined
Sea Ice Temp.		25.0 km	Daily Ascend., Decend., & Combined

Sea ice concentration has been the parameter that is produced routinely from satellite passive microwave data for both global change research and operational requirements. It is the parameter that is used to quantify the extent of sea ice cover, the location of ice edges, the area of open water within leads and polynyas in the ice pack, and the amount of ice that survives the melt season. It is, however, a quantity that is difficult to define because of the ever changing nature, and therefore signature, of the ice cover. For example, as ice evolves from open water through grease ice, nilas, young ice and then thick first year ice with snow cover, the emissivity of the surface also changes constantly from that of open water to that of thick first year ice cover. Thus, in areas of predominantly new ice cover, the retrieved ice concentration can be less that those of thick ice cover, even if the fraction of true open water in both regions are the same. The change is similar to that of the reflectivity of the surface as observed in visible channel data and provide the means to identify areas of interest such as those of polynyas and divergence regions.

Ice temperature, which is a research product, is of great importance for polar studies especially in energy balance calculations. Direct measurement of ice surface temperature is particularly valuable for sea ice cover prediction models (Preller et al., 1992). When combined with ice concentration measurements, ice temperature data would considerably reduce current uncertainties in the estimates of polar energy budgets. The monitoring of long-term changes in ice temperature may also provide valuable information about changes in the thickness of the ice and its snow cover. While AVHRR ice surface temperature algorithms have been developed (e.g., Schluessel and Grassl, 1990; Yamanouchi and Seko, 1992; Comiso, 2000), spatial and temporal coverage is limited by the presence of clouds as noted earlier. On the other hand, passive microwave would provide continuous coverage at good spatial and temporal resolution. It should be pointed out that the parameter retrieved from AMSR represents the snow/ice interface temperature in the seasonal regions and the average temperature of the freeboard layer of the ice in the perennial ice regions.

5.0 Algorithm Description and Theoretical Basis

The basic radiative transfer equation that applies to the brightness temperature, (T_B) observed by satellites at a given wavelength is

$$T_B = \varepsilon T_S e^{-\tau} + \int_0^{\tau} T(z)\ \zeta(z)\ e^{-\tau+\tau'(z)}\, d\tau'(z) + (1-\varepsilon)\kappa\, e^{-\tau} \int_0^{\tau} T(z)\ \zeta(z)\, e^{-\tau'(z)}\, d\tau'(z) \quad (1)$$

where ε is the emissivity of the surface, T_S is the physical temperature of the surface, $\tau'(z)$ and τ are the atmospheric opacities from the surface to a height z and from the surface to the satellite height, respectively, κ is an estimate of the diffusiveness of the surface reflection, and $\zeta(z)$ is the emittance at z. In equation (1), the first term represents radiation directly from the earth's surface which is the dominant contribution. The second term represents satellite observed radiation directly from the atmosphere, while the third term represents downwelling radiation from the atmosphere but reflected from the surface of the earth. A fourth term that takes into account the reflected contribution of radiation from free space, which is a negligible additive contribution, is not included in equation (1).

Within the ice pack, the radiation observed by the passive microwave satellite sensor comes from ice covered surface, open water, or a combination of both. The observed brightness temperature, T_B, is expressed in terms of the relative contribution from each surface by a linear mixing formulation given by

$$T_B = T_O C_O + T_I C_I \quad (2)$$

where T_O and T_I are the brightness temperatures of ice-free ocean and sea ice, respectively. C_O and C_I are the corresponding fractions of each of the two ocean surface components within the field-of-view of the instrument and add to unity (e.g., $C_O = 1-C_I$). Equation (2) forms the basis for sea ice concentration algorithms. The challenge is how to take into account temporal and spatial changes in T_O and T_I which are both functions of emissivity (ε), temperature (T_S), and atmospheric opacities (τ, and τ'), as indicated in equation (1). Such changes can be taken into account or at least minimized through the utilization of several AMSR channels as will be described below.

5.1 Basic Bootstrap Algorithm

Passive microwave data have been especially useful for sea ice studies because of the relatively high contrast in the emissivity of open water and sea ice (Zwally et al., 1983). The contrast is frequency dependent and is higher with the low frequency channels than with the high frequency channels. Thus, if resolution is not an issue, the 6.9 GHz data from AMSR would be best suited for ice retrievals since it provides the best contrast between ice and open water. The radiation at this frequency is also less vulnerable to atmospheric and surface effects than that of the other channels making the frequency channel especially useful for retrieving ice temperatures. The additional use of the 10.7 GHz data is also promising because of better resolution than the 6.9 GHz data and may be utilized to improve the accuracy of the ice concentration retrievals.

Assuming a linear relationship between the brightness temperature and the fraction of ice cover, as in equation (2), the ice concentration, C_I, corresponding to an observed brightness temperature, T_B, over a sea ice covered region can be derived from the equation

$$C_I = (T_B - T_O)/(T_I - T_O). \quad (3)$$

T_O, T_I, and T_B all include contributions from the intervening atmosphere, as described in Zwally et al. (1983). T_I varies spatially mainly because of spatial changes in the emissivity and temperature of the ice, while T_O is approximately constant for open water surfaces within the ice pack. Thus, the success of an ice concentration algorithm depends on how accurately the value of T_I is determined. Equation (3) can be used without correcting each data element for atmospheric effects as long as the atmospheric opacity is relatively uniform spatially for the set of frequency channels that are used in the algorithm. At the frequencies utilized, any advantage provided by an atmospheric correction through a radiative transfer model is usually negated by errors in the model due to the paucity of radiosonde atmospheric data. As will be shown later, the impact of the variability of atmospheric effects on the accuracy of derived sea ice parameters appears to be negligible.

The Basic Bootstrap Algorithm (BBA) is based on the original Bootstrap Algorithm that is currently used for processing SMMR and SSM/I data (Comiso, 1986; Comiso, 1995; Comiso et al., 1997) in which T_I and T_O in equation (3) are determined through the use of multichannel data. Data from three sets of channels have been found to be especially useful: (a) 19 GHz and 37 GHz brightness temperatures, both vertically polarized (called V1937); (b) vertically and horizontally polarized 37 GHz brightness temperatures (called HV37); and (c) 19 GHz and 37 GHz brightness temperatures, both horizontally polarized (called H1937). Scatter plots in 2-dimensional space using the HV37 and V1937 combinations are shown in Figures 1a and 1b, respectively. The data points were collected by a set of P3a aircraft radiometers flown over nearly 100% ice cover in the Arctic in May 1987 (Comiso et al., 1991). In both plots, the data points are mostly along the line AD and form a compact and elongated cluster of points similar in characteristics to those of satellite data (Comiso, 1986). The linearity of the data points along AD is the key information that is utilized by the Bootstrap Algorithm to identify the proper value of T_I in equation (3). In the scatter plot shown in Figure 1a, data points of open water within the pack would fall near the location labeled O. Thus, for an observation corresponding to any data point, B, in this 2-D space, T_I is a data point along the line AD and its value is inferred from the intercept of the lines AD and OB. Ice concentration is determined basically from an equivalent form of equation (3), which in this case is the ratio of OB to OI, as described in Comiso (1995). The complete formulation is given in Comiso (1995) and explicitly in the next section but with brightness temperature data replaced by emissivity data. The existence of consolidated ice clusters such as those along AD in Figure 1 have been confirmed by ship radiometer data over the Antarctic (Comiso et al., 1989; Grenfell et al., 1994) and over locally grown sea ice at CRREL (Grenfell and Comiso, 1986). The variability of the data points across the consolidated ice cluster defined by the line AD in the similar scatter plots that make use of satellite data is a measure of the variability of T_I and includes temperature, emissivity, and atmospheric effects.

In the Arctic, a combined used of the HV37 and V1937 sets is desirable because of spatial inhomogeneity and complexity in the physical characteristics of the ice cover (Comiso, 1986). The use of the HV37 set is especially advantageous in the perennial ice region in winter, because the slope of data points in this set is close to unity and hence the temperature effects are minimal. Also, the standard deviation of data points about the line AD is close to 2K which is equivalent to 2.5% error in the estimates of ice concentration. This reflects how well sea ice concentration can be derived in the region. The V1937 set is a good complement of the HV37 set and has the advantage that it uses vertical channel data only which are observed to be less affected by layering and inhomogeneities in the ice (Matzler, 1984; Grenfell et al., 1994) than the horizontal channels. This set has been found to be especially suitable in seasonal sea ice regions as in the peripheral seas of the Arctic and most part of the Antarctic (Comiso et al., 1984; Comiso and Sullivan, 1986) where snow cover is known to have layering and a very complex texture (Massom et al., 1998; Worby and Massom 1995).

Although the V1937 set is more sensitive to fluctuations in ice temperature than the HV37 set (Comiso, 1995), the spatial variations in surface ice temperature (i.e., snow ice interface temperature), as observed from limited data in the Antarctic, has been observed to be relatively small and have a standard deviation of about 2K. Sensitivity studies and analysis of the distribution of the consolidated ice cluster indicate that the error from temperature effects is indeed small compared to other sources of error. In the Antarctic, the HV37 set is not as useful as in the Arctic because consolidated ice data in this set are close to or almost along the line OA. The use of this set would lead to the retrieval of erroneously large fraction of open water in some consolidated ice regions. The V1937 set has thus been the primary set used to retrieve ice concentrations from SMMR and SSM/I data. Recent studies, however, indicate that the accuracy of the retrieved product in the Antarctic can be further improved with the use of a formulation similar to that of the Arctic but with the H1937 set used instead of the HV37 set. The additional use of the H1937 set has been observed to be especially useful in young ice regions and enables a better characterization of the sea ice cover near coastal and polynya areas. The use of the latter is a new and is currently part of the Basic Bootstrap Algorithm.

Typical monthly sea ice concentration maps derived using BBA for the Northern and Southern Hemispheres during summer and winter are shown in Figure 2. The large seasonal change in the extent of the ice cover in both hemispheres are apparent. Also apparent are relatively lower concentrations than average along coastlines, which are sites of coastal polynyas, near islands and big icebergs, and along the ice edges. These regions are sites of open water and new ice. The maps thus represent what is generally expected as ice distributions in both hemispheres.

5.2 The AMSR Bootstrap Algorithm

The AMSR algorithm for sea ice is a modified version of the Basic Bootstrap Algorithm and is called the AMSR Bootstrap Algorithm (ABA). The modified version will provide the means to estimate surface ice temperature and at the same time use the latter to further reduce errors in the determination of ice concentration. In particular, it makes use of 6.9 GHz data to reduce if not eliminate temperature effects when the V1937 and H1937 data sets are utilized. The algorithm has been successfully tested using SMMR data which have the basic channels required. However, some adjustments would be needed after launch when real AMSR data becomes available since SMMR is known to have problems with calibration and the resolution of the 6 GHz channels is coarse at 150 km, compared to 58 km for AMSR.

The schematic of the procedure for estimating of ice concentration and ice temperature, is shown in Figure 3. The technique which was reported in Comiso and Zwally (1997) is similar to that of the Basic Bootstrap Algorithm, as described in Comiso (1995), with T_B replaced by ε, the latter basically independent of temperature fluctuations. The effective emissivity of the surface within each data element can be estimated from

$$\varepsilon_B = \varepsilon_I C_I + \varepsilon_O (1-C_I) \quad (4)$$

where C_I is initially obtained from equation (3) through the use of a combination of 6 and 37 GHz channels at vertical polarization, while ε_I and ε_0 are emissivities of ice and open water, respectively, which can be derived from histograms of data within the pack and assumed constant. Unlike equation (2), equation (4) is not the exact formulation for the observed satellite data but sensitivity studies indicate that the associated error is very small (<1%) and is highest when the concentration is 50%. The physical temperature of the ice surface within each data element is then given by

$$Tp = T_B (6V)/\varepsilon_B(6V) \quad (5)$$

where $T_B(6V)$ is the observed brightness temperature of the surface at 6 GHz (vertical polarization). The emissivity of the surface at 19 and 37 GHz can then be derived from

$$\varepsilon_B(19V) = T_B(19V)/Tp \quad (6)$$

$$\varepsilon_B(19H) = T_B(19H)/Tp \quad (7)$$

$$\varepsilon_B(37V) = T_B(37V)/Tp \quad (8)$$

and

$$\varepsilon_B(37H) = T_B (37H)/Tp \quad (9)$$

with the assumption that the temperature of the layer of ice from which radiation emanates is approximately frequency independent between 6 and 37 GHz and is equal to Tp. The use of emissivity instead of brightness temperature for estimating ice concentration is justified by the matching of reference data points of both consolidated ice (100% IC) and open water (0% IC) as discussed in Comiso and Zwally (1997). As in Comiso (1995) which makes use of brightness temperatures, the tie points for a datapoint at B are represented by the intercept points (ε_{1I},ε_{2I}) along the 100% ice line AD which are calculated using the equations

$$\varepsilon_{1I} = (\varepsilon_{1A} - \varepsilon_{1O} - \varepsilon_{A2} S_{AD} + \varepsilon_{2O} S_{OB})S_{OB} /(S_{OB} -S_{AD})+ \varepsilon_{1O} - S_{OB}\varepsilon_{2O} \quad (10)$$

$$\varepsilon_{2I} = (\varepsilon_{1A} - \varepsilon_{1O} - \varepsilon_{2A} S_{AD} + \varepsilon_{2O} S_{OB})/(S_{OB} -S_{AD}) \quad (11)$$

where S_{AD} and S_{OB} are slopes of the lines AD and OB, respectively, (ε_{1A} , ε_{2A}) represents any point along the line AD, and (ε_{1O} , ε_{2O}) represents the open water reference emissivity. The ice concentration for the data point at B is derived from the ratio of the distances OB and OI (see Figure 1) and given by the equation

$$C = [\{(\varepsilon_{1B} - \varepsilon_{1O})^2 +(\varepsilon_{2B} - \varepsilon_{2O})^2 \}/\{(\varepsilon_{2I} - \varepsilon_{2O})^2 + (\varepsilon_{1I} - \varepsilon_{1O})^2 \}]^{1/2} \quad (12)$$

In the formulation, it is convenient to choose ε_{2A} =0 at point A along AD with ε_{1A} the resulting offset. Additional details, including the assumptions in the determination of the line AD and the point O, are discussed in Comiso (1995). Since the initial calculation of the emissivity at 6.9 GHz makes use of ice concentration that has not been temperature corrected, the emissivity is recalculated using the more accurate result from equation (12) and a second iteration follows, starting with equation (4) as indicated in Figure 2, to obtain the final ice concentration estimate. Also, the final value of Tp is then used to calculate the average physical temperature of ice surfaces in each data element, T_S, using the equation

$$T_S = [T_P - T_O(1-C_I)]/C_I. \quad (13)$$

To illustrate the effectiveness of ABA, we make use of SSM/I data in conjunction with skin surface temperatures derived from AVHRR data (Comiso, 2000) since the former do not have a 6.9 GHz channel. Figures 4a-4d show examples of skin surface temperature maps for a summer (March) and a winter (September) month in 1992 in both hemispheres. The images show temperature distributions over the open water, sea ice, and the continent and illustrate how surface temperature changes spatially at various latitudes. As expected, the coldest temperatures are located in the continent while intermediate but still subfreezing temperatures are over sea ice with the temperatures increasing progressively towards the north. Areas of polynya formation are usually warmer than adjacent regions. These temperature data are then converted to snow/ice temperature data, that would represent T_P in the above formulation, using regression parameters derived by Comiso et al. (1989) using data in the Antarctic region.

To illustrate the difference between the use of brightness temperatures alone compared with the use of emissivity, Figures 5 show scatter plots using the HV37 and V1937 sets for both variables in the Arctic region during winter. The distributions for brightness temperatures are shown to be very similar to those of emissivities. The cluster along the consolidated ice (AD) are also shown tobe equally compact. Although there are large spatial variations in surface temperature as indicated in Figure 4, the net effect on the distribution of the data points in the HV37 and V1937 sets appears to be small.

In the consolidated ice regions, the data points are apparently redistributed such that the net variability about the cluster AD in the emissivity plots is essentially the same as in the brightness temperature plots. This implies very similar errors for both systems. Similar plots are shown in Figure 6 for the Antarctic. Again the brightness temperature plots are very similar to those of the emissivity plots.

Ice concentrations were derived using T_P from AVHRR and ABA for the same summer and winter months of 1992 (as in Figure 2) and the results are presented in Figures 7a-7d. The maps for each season look very similar with the areas of high ice concentrations and reduced concentrations confined in the same general locations. The ice concentration maps for September 1992 in the Antarctic have been shown to be consistent with Landsat and OLS satellite observations (Comiso and Steffen, 2001), and with the expected behavior of the ice cover in coastal and some deep ocean regions (e.g., near the Maud Rise and the Cosmonaut Sea) where polynyas have been observed. Difference maps between the BBA and ABA ice concentrations for each season are shown in Figures 8a-8d. Generally, the two maps are basically identical within errors. Relatively higher concentrations (by less than 4%) are observed with the ABA in the Central Arctic and near the continent in the Antarctic region where the difference are likely due to much colder temperatures than average. It is interesting to note, however, that alternating positive and negative differences are observed around the periphery of the Antarctic ice cover. This is coherent with the effect of the Antarctic Circumpolar Wave (ACW) as described by White and Peterson (1996) in which alternating high and low temperature anomalies are observed. The advantage with ABA, is that it enables the retrieval of surface ice temperatures, and has the potential of obtaining more accurate retrievals in coastal polynyas and in regions where the surface ice temperatures are abnormally cold. The difference from the two retrievals may be small but for some regions, like polynya regions, the impact may be significant.

Since low frequency channels are not available in the SSM/I system, ABA was also developed and tested using Nimbus-7 SMMR data. The SMMR system, which has a 6.6 GHz channel, provided the means to put together a working version of ABA that has the right input parameters. However, the effectiveness of ABA, especially in retrieving ice temperatures, could not be fully tested because of very large footprints for SMMR and instrumental problems associated with polarization mixing. This made it difficult to evaluate discrepancies between BBA and

ABA results. The advent of AMSR data and the validation program will provide the means to test and refine the program and validate the results.

5.3 Masking Algorithms

Since the polar maps include land areas, a land mask is used to ensure that the algorithm is applied on data in the ocean regions only. Previous versions of such land mask have been based on existing maps put together through collaborative efforts of many agencies and foreign countries but the accuracy in some areas have been questionable because of the lack of direct measurements in these areas. Such mask has been updated using data from a dedicated RADARSAT mission in the Antarctic in 1998. Significant differences between the old and the new maps are apparent, reflecting some errors in the previous data and a constantly changing continental boundary due to surges and iceberg calving. The comparison indicates that surges at the Ross Ice Shelf and Ronne Ice Shelf have been going on in the last few decades. If the previous land mask currently used for SSM/I data is used on recent data, it would produce erroneous coastal polynyas of about 50 km wide. It is apparent that the location of the continental margin is not constant and that regular updates in the land mask for sea ice retrievals is needed.

At the ice-free land/ocean boundaries, there are also erroneous ice concentrations in the ocean part adjacent to land because the brightness temperatures are similar to those of ice covered regions. To illustrate this problem, an ice concentration map in the Ross Sea region is shown in Figure 9a during the summer when the Ross Sea Ice Shelf boundary has a minimum of sea ice. Along the continental boundary, significant ice cover is retrieved by the algorithm. The result for applying an algorithm developed by Cho et al. (1996) is shown in Figure 9b. The technique uses a running 3 by 3 matrix with the middle pixel in consideration. If there is a land pixel in the matrix, the middle pixel value is replaced by the minimum value within the 3 by 3 matrix. The technique is effective in removing some of the pixels with non-zero ice concentration in the north and western side but overall, improvements appeared to be needed. An improved version of this technique is currently used for the Bootstrap algorithm and when applied, the result is shown in Figure 9c. This later technique which searches one or two pixels further to find open water generally better results than the Cho et al. technique, as indicated, but at the front of the ice shelf, there is still significant ice. Generally, it works better in other regions but for this particular case, it did not work very well because of aforementioned problem with the land/ocean mask. The ice covered area in front of the shelf is more than should be the case because the actual front of the shelf is further north than indicated by the land mask (white). The latter technique is more effective when there is less contamination along the coastline, as is usually the case, and also when AVHRR climatological temperature data are used to mask out areas in relatively warmer oceans.

The retrieved ice concentrations also show erroneous data in areas of open ocean where the signature is similar to those of ice covered ocean. This usually happen in areas of abnormal weather and/or wind conditions. A masking technique to automatically eliminate such bad data in the open ocean has been developed,as described in Comiso (1995), but such technique is not 100% efficient, especially with SSM/I because the lowest channel is close to the water vapor line. The use of the AVHRR climatological data in conjunction with the ocean masking technique provide significant improvements but not near the sea ice margin. The use of low frequency AMSR data, which are less sensitive to weather effects (e.g., 6.9 and 10.7 GHz) and show better contrast between sea ice and open water are expected to significantly reduce errors in the marginal ice region.

5.4 Error Analysis and Sensitivity Studies

The physical basis of and assumptions in the Bootstrap algorithm have been confirmed using ship based radiometer experiments in the Antarctic (Comiso et al., 1989; Grenfell et al., 1994), an aircraft experiment in the Arctic (Comiso et al., 1991) and a controlled sea ice experiments at the Cold Regions Research Laboratory (Grenfell and Comiso 1986). Comparative studies of ice concentrations derived from SSM/I using the Bootstrap Algorithm with those derived from aircraft, SAR, Landsat, and helicopter data have indicated consistencies within an average of 5 to 15% in winter and 10 to 20% in the summer (Comiso et al., 1984; Comiso, 1986; Comiso et al., 1991; Comiso and Kwok, 1996; Comiso and Steffens, 2001). Good validation data sets for much of the Antarctic region, however, have been difficult to come by and hence the need for a coordinated aircraft and in situ validation program in the region, especially for a new and more versatile system like AMSR.

Errors associated with the estimate of ice concentration are caused primarily by spatial and temporal changes in surface temperatures, emissivity, and atmospheric opacity. Other sources of errors include the retrieval of erroneous ice concentrations in the open ocean and at the land/ocean boundaries as discussed in the previous section. The impact of surface temperature has been examined and discussed previously. It is apparent that the maps generated with BBA and with ABA, provide results that are almost identical within errors. Sensitivity studies for errors due to variations in temperature has also been reported previously (Comiso, 1995; Comiso et al., 1997). Because the snow cover is such a good insulating material, the spatial fluctuation of the snow/ice temperature has been found to be relatively small (with σ being about 2.5 K). The Antarctic sea ice cover is very seldom without a snow cover not only because of frequent snow precipitation but also because of drifting snow. However, katabatic and geostropic wind can be persistent in some areas, depleting the snow cover and causing the temperature of the emitting sea ice surface to be abnormally low in some regions of Antarctica. The difference maps in Figure 4 show that in these regions, the average bias due to temperature is about 2 to 4%. This discrepancy is small but if verified to be indeed a bias associated with temperature, the use of ABA provides enhanced ability to characterize more accurately small features of scientific interest, such as coastal polynyas, the sizes of which are sometimes comparatively small.

The large variability in the emissivity of the sea ice cover (Grenfell et al., 1994) is likely the main source of error in the determination of sea ice concentration. The success of the algorithm depends on the ability to establish the right tie-point (T_I) for each data element. Cluster analysis results indicate that most of the data points representing 100% ice cover tend to cluster along the line AD in Figure 1. This information enables the algorithm to account for the large variability in emissivity (and also in temperature and atmospheric opacity). The algorithm assumes that the cluster is approximately linear. Any significant deviation of an ice data point from this linearity and the location of the AD line produces an error. Also, the accuracy in the retrieval depends on the compactness of this cluster along the line AD.

In the Arctic, the distribution of the data points in the HV37 and V1937 sets are shown in Figure 5a and 5b for brightness temperatures and Figures 5c and 5d for emissivities. In the Central Arctic, the data points have a standard deviation of about 2 K about this line for the HV37 set which is the main set used in the region. In the Antarctic, the scatter plots for H1937 and V1937 are shown in Figure 6 and indicate less defined distributions along AD than those in the Arctic. The standard deviation about the cluster line is higher at about 5K for the V1937 set which is previously the only set used in the region. The error in the determination of ice concentration is thus higher in the Antarctic than in the Arctic.

Polarization and gradient ratios have been used in the NASA Team Algorithm to overcome spatial variations in surface ice temperature. The use of this technique, is apparently not so effective in the seasonal ice region, especially in the Antarctic, because of possible differences in the response of the vertically and horizontally polarized radiation to different surface and subsurface conditions within the ice pack can be very different (Markus and Cavalieri, 2000; Comiso and Steffen, 2001). The results is also an indication that variability in emissivity is indeed a much bigger source of error than variability in ice temperatue.

Depending on frequency, the emissivity of first year sea ice can be very different from that of multiyear ice. This is especially the case in the Arctic because of the presence of an extensive perennial ice cover. In the Antarctic, the signature of multiyear ice is more difficult to establish. At the end of the summer, the region with the largest area of sea ice cover is located in the Western Weddell Sea. However, the signature of ice in this perennial ice region is similar to that of most other Antarctic regions (Zwally et al., 1983). The reason for this is that the summer ice is actually advected to the northeast during the subsequent winter following the direction of the Weddell Gyre and causing the ice cover in the Western Weddell region to be eventually replaced by seasonal sea ice during the year. However, in other areas like the Bellingshausen/ Amundsen (B/A) Seas, the signature of ice in the winter is different from those of other regions. This was most apparent in the 1980s when the region was consistently covered by perennial ice during the summer. Unlike the ice cover in the Western Weddell region, the perennial sea ice at B/A are more confined and could remain basically in the same general location for several years and therefore acquires a multiyear ice signature as in the Arctic. To minimize the error in the retrieval of ice concentration in the region, a different tie point for consolidated ice (i.e., different slope and offset for AD) is used to better match the different distribution of ice clusters in the region. Such correction is necessary since otherwise, large areas of the region would be mistaken as a divergence or polynya regions. Since 1989, however, drastic retreats in the summer ice cover was observed (Jacobs and Comiso, 1994), due to a

possible change in the climate of the region (King and Harangozo, 1998). In 1989 and later dates, it became evident that the signature of ice in the B/A region is more and more similar to those of the rest of the Antarctic region likely because of gradual disappearance of thick multiyear ice cover. While not a serious problem at present, AMSR data will be examined for changes in the ice distribution patterns that may cause multiyear ice signatures in some areas to reappear again.

The signature of sea ice in the spring and summer also becomes very different from that of autumn and winter. This happens as a result of wetness in the snow cover due to above freezing temperatures during the period. When the snow cover has about 3% liquid water, as in early spring, the dielectric property of the surface becomes very high and the snow surface becomes opaque. The resulting emissivity of the surface approaches that of a blackbody and the observed brightness temperature of sea ice at all frequencies increases considerably. As spring progresses, the snow gets melted and the surface of the ice is covered by slush or liquid causing an effect that is opposite to that of early spring. The emissivity of ice during this period is thus not as well defined as during the winter period. Errors in the retrieval of ice concentration are therefore larger and adjustments in the tie points are desired to account for the changing character of the surface and to optimize accuracy.

The ocean mask can also be a source of error if it does not provide consistent lower threshold for ice concentration. This threshold is established for some average conditions but algorithms for the ocean mask may not be able to adjust to big fluctuations in weather and wind conditions. At some low concentration levels, it is difficult to discriminate between sea ice covered area and open water because the brightness temperatures for these two types of surfaces are almost identical. The lowest (threshold) ice concentration in which discrimination is possible is what normally defines the ice edge location. For SSM/I, the discrimination is done through the use of a cut-off in the V1937 and V1922 sets, as described in Comiso (1995). While this may improve with AMSR data, the threshold concentration currently used is approximately 10% but for better consistency, a 15% cutoff is usually used for long term ice extent studies. The cut-off technique is basically effective, as illustrated in the comparison of an ice concentration map derived using the Bootstrap algorithm and a SAR image for the region indicated by a rectangular box in the ice concentration map (Figure 10a). Features at the ice edge shown by the high-resolution SAR image are basically reproduced in the passive microwave image. The open water features within the ice pack are also coherent in the two images if the changing SAR backscatter for open water within the ice pack is taken into account. It is also apparent in Figure 10b that the character of the ice cover changes significantly from the marginal ice zone, where loosely connected pancakes, new ice, and ice bands are located, to the inner zone, where thicker and more consolidated ice are found.

A more quantitative characterization of the ice edge by satellite data is depicted in the plots in Figure 11. The plots in Figures 11a and 11b represent brightness temperatures at 6 SSM/I channels along a transect at approximately 148 ^{o}E longitude from open water through the marginal ice zone and into the pack. As indicated, the brightness temperature increases with latitude at all frequencies except at 85 GHz (vertical polarization) in the marginal ice zone. The approximate location of the ice edge along this particular transect has been provided through direct observations from the Australian ship, R.V. Aurora Borealis, and is represented by the vertical dash line. The ice concentrations derived from the Bootstrap and Team algorithms are indicated in Figure 11c and shown to increase with brightness temperatures and have values of about 25% at the ship observed ice edge. Ship observations are usually dependable but difficult to interpret in terms of large scale characteristics in the ice cover because of limited field of view. Complications in the observation of the ice edge can be seen in the SAR image (Figure 10b) in which ice bands form and grease ice can form several kilometers beyond (to the north of) the ice bands.

While the specific case shown in Figure 11 indicates good agreement, some other cases, reported in Worby and Comiso (2001), show large discrepancies. Sometimes, the ice edge identified from ship is several km to the north of the SSM/I ice edge. This is especially the case in spring and summer, when ice floes breaks up and the surface of the ice is covered by liquid. Also, sometimes the opposite is true, and this is usually the case when the ship misses some ice fronts to the north, as in the SAR image. Furthermore, the ice edge location, as identified by the Bootstrap algorithm, is sometimes several km to the north of that identified by the Team algorithm. For long term time series studies, consistency in the determination of ice extent is important and this can happen only if the ice edge is identified in a consistent manner for each season and independent of weather, and satellite sensor.

Errors associated with the spatial and temporal variability in the opacity of the atmosphere are expected to be

small at microwave frequencies used by the algorithm and are often neglected [*Comiso and Zwally*, 1982; *Massom*, 1991]. However, some sensitivity studies using a radiative transfer model have indicated that such errors can be as large as 10% when the Team Algorithm is used [*Oelke*, 1997]. Not knowing how accurately the models represent actual conditions and what the effect is on the Bootstrap algorithm, actual data are used to investigate the impact of the passage of a low pressure system in the Ross Sea region on derived daily ice concentrations. Figures 12a and 12b show ECMWF mean surface pressure maps and synoptic winds during two periods (June 13 and June 20) when there were large changes in the pressure fields. Figures 12c and 12d are scatter plots of 19 GHz(V) versus 37 GHz(V) data in the region shown in the other images while Figures 12e and 12f show corresponding ice concentration maps. Comparing ice concentrations in the rectangular box shown in the images, which includes the low pressure field in June 20th, the Bootstrap algorithm yielded an average ice concentration of 97% with a standard deviation of 2.7% on June 13 and an average ice concentration of 98% with a standard deviation of 2.1% on June 20. For comparison, the Team algorithm yielded an average ice concentration of 90% with a standard deviation of 5.5% on June 13 and an average ice concentration of 86% with a standard deviation of 3.4% on June 20. These results indicate that the impact of the passage of a low pressure system on the daily ice concentration in relatively consolidated ice regions was relatively minor, especially for the Bootstrap algorithm. In the scatter plots, data points within the rectangular study area are shown as red and it is apparent that the occurrence of the low pressure system caused the brightness temperatures to increase slightly (suggesting enhanced emission in the atmosphere) but proportionately at the 19 and 37 GHz channels. The ice concentrations did not change much because the increases caused the data points to shift along the line AD, which correspond to the tie points for consolidated ice in the Bootstrap Algorithm. It should be noted that winds were relatively steady during the two periods in the study area but a much stronger change occurred at the Ross Sea shelf region (at about 77^{o} S, 180^{o} E) likely causing the observed reductions in concentrations in the region from June 13 to June 20. A seven-day separation was chosen to ensure that atmospheric conditions over the pack ice were different. A similar study with 3-day separation (June 17 and 20) yielded very similar results.

5.5. Validation Issues and Validation Program

The validation criterion is that the derived AMSR-E sea ice products agree on average with the corresponding validation data set to within the estimated accuracy of the validation data set. The validation data sets will be derived from any or a combination of field, aircraft, submarine and high-resolution visible and infrared satellite data and are expected to provide a more accurate measure of the standard sea ice products than the AMSR retrieved products. The underlying philosophy of this approach is that confidence in the sea ice products derived from the AMSR will be achieved by showing consistency of such products with independently derived data that are spatially and almost temporally coincident (Comiso and Sullivan, 1986; Cavalieri, 1991; Cavalieri et al., 1991; Steffen and Schweiger, 1991; Grenfell et al., 1994). Operating within this paradigm, the following is a summary of validation methods for each of the AMSR standard products.

The cornerstone of the validation program is the acquisition of a comprehensive data set after the launch of ADEOS-II and EOS-Aqua satellites. The data set will consist primarily of concurrent aircraft, in situ, and satellite data to be collected during the winter 2003 and spring 2004 periods in both hemispheres. One such dedicated program is the Antarctic AMSR Validation Program sponsored by NASA. A P-3 aircraft equipped with a scanning microwave radiometer which has all AMSR frequencies, an infrared radiometer, a laser altimeter and a snow radar will be used on a mission based in Punta Arenas, Chile in August 2003. A sample track for the aircraft over ice covered ocean is shown in Figure 13. Cruises that are expected to provide in situ data during the validation period include those for the US/Nathaniel Palmer, the UK/HMS Endurance, the German/RV Polarstern and other international vessels. Among the polar scientists who had expressed interests in this validation endeavor are Dr. F. Nishio of Japan, Dr. Doug Martinson and Stan Jacob of Lamont Earth Science Observatory, Prof. Koni Steffen of the University of Colorado, Dr. Miles McPhee of the University of Washington, Prof. Ray Smith of the University of California at Santa Barbara, Dr. Peter Wadhams of the University of Cambridge and Dr. Martin Jeffries of the University of Alaska. The validation program will be coordinated with related projects, especially activities of other scientists whose proposals were approved under a general validation program for the ADEOS-II and EOS/AGUA project and under various Announcements of Opportunities in the Earth Science Enterprise Program. The strategy is to take advantage of in situ and other data sets that will be available for this time period. Similar projects will be undertaken with ships of opportunities that will be in the Arctic and Antarctic region during the validation period. Issues and strategies for validating sea ice concentration and ice temperature are discussed below.

Sea Ice Concentration: Sea ice concentration is defined as the areal percentage of sea ice observed within the field of view of the satellite sensor. The primary approach for the validation of retrieved AMSR ice concentrations is to utilized data from the dedicated aircraft campaigns in conjunction with high resolution satellite data, including those from Landsat 7, Terra and Aqua MODIS, NOAA-AVHRR, DMSP-OLS, RADARSAT. The aircraft data will provide the means to assess the absolute accuracy of the retrieval at some places and some seasons while the satellite data provides better spatial and temporal coverage. High-resolution active microwave satellite data such as the Radarsat SAR, are most useful during persistent cloud cover conditions and during darkness. Data from microwave scatterometers, such as those from QuickSCAT, will be utilized for identifying areas of divergence and where significant reductions of ice concentration is expected. However, data from active systems are more difficult to interpret than those from passive and visible systems, because of unpredictable backscatter from different ice types, from open water within the ice pack, and from wind-roughened seas. Such data are valuable but require validation.

Aircraft campaigns are planned for both Arctic and the Antarctic regions and for dry and wet seasons. Such program will provide multi-channel passive microwave data similar to AMSR but at a much better resolution. The high resolution will provide the means to test the effectiveness of the mixing formulation in different ice regimes and conditions. The aircraft will also be equipped with digital and film camera system for the characterization of small features of the ice cover, a laser ranging system for surface topography studies and ice thickness estimates, and a multi-frequency radar for snow cover studies. The strategy is to apply the algorithm on co-registered and coincident aircraft and spacecraft data and evaluate how the results matches each other quantitatively and how they compare with similar analysis from high resolution visible and infrared data. Discrepancies will be analyzed and explained through the use of ancillary data and further examination of the high resolution data. Data at the ice edge, open ocean, and land/ocean boundaries will also be analyzed to validate the effectiveness and consistency of the masking algorithms.

The validation program will take into consideration the large changes in physical and radiative characteristics of sea ice during an ice season. During early ice growth period, the ice cover consists mainly of new ice, pancakes, young ice, and relatively undeformed first year ice. On the other hand, during late winter, the ice cover consists of predominantly thick and vast ice floes with relatively thick snow cover. During the melt season, the vast ice floes get broken up to smaller units and the surface gets covered by slush or liquid. For at least two periods (dry and wet periods) the changes in the radiative signature will be quantified as accurately as possible and relationships with the accuracy of the retrieved sea ice parameters will be evaluated.

As a complementary approach, time series of images will be analyzed to check AMSR retrievals for temporal consistency. The growth and decay of sea ice are limited by physical laws and environmental conditions and such time series data can provide the means to establish how well the expected time development of the ice cover is reproduced by the satellite data. This effort will help identify weaknesses in the technique that are not obvious from examination of individual images.

Atmospheric effects can be estimated using radiative transfer modeling to account for the effects indicated by equation (1). The results from the latter can be used to correct the brightness temperatures observed by the aircraft and satellite and results are used to derive the geophysical parameters that are used in the validation. As indicated earlier, the choice of channel is important and with the set of channels used in the ABA algorithm, the effect appears to be negligible. Further confirmation that this is indeed the case will be done through radiative transfer modeling studies of atmospheric effects using actual atmospheric profile measurements during the validation period.

Radiative transfer modeling of the microwave radiation emanating from the sea ice cover will also be undertaken because it allows for a better understanding of the emission characteristics of different sea ice surfaces at the different AMSR frequencies and polarizations. Such procedure has been conducted previously (e.g., Tjuatja et al., 1993; Grenfell et al., 1994; Tjuatja et al., 1995) but results were of limited value because of the lack of needed atmospheric and surface data. Some refinements will be implemented and data acquired during the validation program will be used to obtain improved results that will be used to better interpret spatial and temporal changes in the microwave signatures as observed in the aircraft, field, and satellite data sets.

Sea Ice Temperature: The ice temperature derived from the vertically polarized 6.9 GHz channel represents the temperature of the sea ice layer that emits much of the signal observed by the radiometer. For first year ice, it is the temperature of the snow/ice interface because at this frequency the snow cover is transparent to the radiation and the surface is opaque due to relatively high salinity. For multiyear ice, the derived sea ice temperature represents a weighted-average of the freeboard portion of the ice. During previous Antarctic cruises, the physical characterization of the ice cover made on a regular basis included quantitative measurements of temperature profiles through the snow and ice. Such data were taken during the Weddell Sea winter and spring cruises of 1982, 1983, 1986, and 1989. These data were used to obtain empirical relationships between the snow skin-depth temperatures and the snow/ice surface temperature. The snow skin-depth temperature is routinely measured by infrared (IR) satellite instruments (e.g., AVHRR, ATSR, and MODIS). The primary technique for the validation of AMSR ice temperature data is to make use of this empirical relationship that converts IR satellite data to ice temperature data and use the latter for comparative analysis with AMSR data. The aircraft IR data will be converted to surface ice temperatures that in turn will be compared with ship measurements to assess errors associated with the use of empirical parameters. Further refinements of the empirical parameters will be made through the use of more field data and a thermodynamic model of sea ice and snow.

The retrieved ice temperatures will be further validated using surface temperature data from buoys, ships, ice camps, and other platforms. While these are only point measurements, the horizontal variability of the snow/ice interface temperature is not expected to be large over a few km. Also, there exist some arrays of buoys that provide continuous measurements and could be used to check the temporal consistency of the derived AMSR temperature data.

6. Computer Requirements and Coordination

6.1 Software and Data Storage Requirements

The Basic Bootstrap algorithm (BBA) has been tested without problems at the NASDA Earth Observation Center data facility and is ready for routine processing. An enhanced version of this algorithm has been enhanced to better account for spatial variations in surface ice temperature as described in this document. The new algorithm is called AMSR Bootstrap Algorithm (ABA). This algorithm has been tested using SMMR data but AMSR data is expected to be much better calibrated and has much higher resolution than SMMR. Further testing is thus necessary once AMSR data becomes available. In the meantime, BBA can be used since results from the two are very similar and the differences where they occur are within errors. Both algorithms have working versions currently running on SGI UNIX workstations at Goddard. ABA is only a slightly bigger program than BBA and there should not be any problem installing it in the NASDA system. An estimate of processing time for one month of SSM/I Level-3 daily average data is of the order of 1.2 minutes and 2.1 minutes on an SGI Octane workstation using BBA and ABA, respectively.

Input to the AMSR-E sea ice algorithms will consist of Level 2A AMSR brightness temperatures, latitude, longitude, time and a land/ocean flag. The output sea ice products will consist of sea ice concentration and sea ice temperature and will include latitude, longitude, and a time stamp. The algorithms are coded in C. As soon as AMSR data is available, ABA will be tested and a final version including documentation will be delivered to NASDA within a few months.

6.2 Data Management, Quality Control and Archival

The NASDA/Earth Observation management is primarily responsible in the acquisition and management of AMSR data. During the first year of operation, AMSR data will also be processed by the PI, using his own computer system, for comparative analysis with other data sets and for quality control. Enhanced techniques and procedures developed during this time will be delivered to NASDA for implementation and generation of the sea ice data sets.

Quality control of brightness temperatures will be done during the generation of the Level 2A products. The first step in the quality control of the sea ice products will consist of checking whether or not the retrieved sea ice products fall within reasonable limits. Diagnostics will be based in part on satellite sea ice climatology developed since the launch of the Nimbus 7 SMMR in 1978. These data will provide a useful measure of the seasonal and regional values for sea ice concentration and to some extent sea ice temperature.

Exception handling will consist of flagging missing data, land, and unreasonable retrievals. Missing brightness temperatures will result in setting a missing flag for the sea ice retrieval. The sea ice algorithm will not be run over land. It is presumed that out-of-range brightness temperatures will be handled in the generation of Level 2A products. Out-of-range retrievals will be handled within the algorithm. Diagnostics for checking out-of-range data will be used in the algorithms to determine whether the output should be flagged as unreasonable. In some cases, for example, sea ice concentrations greater than 100% will be set to 100% and sea ice concentrations less than 0 will be set to zero. Much larger discrepancies will be flagged as unreasonable.

6.3 Consistency Checks and Coordination with Other Projects

Sea ice concentration and ice temperature are two parameters that are obtainable using other satellite sensors. For example, one of the data products that are supposed to be generated from ADEOS-II/GLI and EOS-Agua/MODIS is sea ice concentration using visible channel data. There may be differences in sampling rate, resolution and sensitivity to clouds and weather but where there is good cloud free data available from GLI and MODIS, the retrieved product should agree with that of AMSR. Also, GLI and MODIS sensors have thermal infrared channels that provide surface skin temperatures. After a normalization is applied to the latter, to obtain ice temperature, as discussed earlier, the results should be compatible with ice temperatures derived from AMSR. If not, the reason for the discrepancies should be evaluated in terms of different resolution, different emissivities and reflectivities, and different types of surfaces. Retrieved geophysical parameters should be sensor independent but if the results from different sensors are different, users of the products should be advise about such differences and why.

Validation data are oftentimes very expensive to acquire and should be shared with other projects which might need them. Among the key validation data sets that will be used for AMSR data are the aircraft and Landsat data as described earlier. The same data sets could also be used for validating GLI and MODIS products. Similarly, validation data sets accumulated for GLI and MODIS may be useful for AMSR data validation.

Activities of the scientists and engineers involved in different projects should also be coordinated such that the same set of standards are applied to different sensors, especially those that are similar. For example, AMSR data from both ADEOS-II and EOS-Aqua should be processed with the same quality checks and calibration standards. Similarly for aircraft radiometer AMSR simulator data that need to be compared with satellite data. This will guarantee that data sets from different sensors are consistent and can be used interchangeably and/or in combination for scientific research.

7. Summary

The theoretical basis and description of the algorithm that will be used to derive sea ice parameters from AMSR data has been discussed. Two techniques with almost equal performance are presented. One is called the Basic Bootstrap Algorithm (BBA), which is the original algorithm that was proposed to NASDA for evaluation and was chosen to be used as the standard algorithm for AMSR. An enhanced technique has been developed in the meantime and called AMSR Bootstrap Algorithm (ABA) which is expected to provide more accurate results. The two algorithms, as tested, are currently providing very similar results but ABA has the advantage of accounting for abnormally cold ice surface temperatures and in providing an ice temperature product. The latter is a research product but could provide very valuable information needed for polar process studies that cannot be obtained otherwise. The error in the determination of ice concentration is estimated at about 5 to 15% during winter and 10 to 20 % during the summer using SSM/I data. This significantly improves when AMSR data is used since the latter have much better resolution and greater spectral range. The error in the determination of ice temperature is yet to be determined but is expected to be less than 4K.

8. References:

Aagaard, K., L. K. Coachman, and E. C.mack, On the halocline of the Arctic ocean, *Deep Sea Res.*, 28, 529-545, 1981.

Badgley, F. I., Heat budget at the surface of the Arctic Ocean, in Proc. of the Symp. on the Arctic Heat Budget and Atmospheric Circulation, J. O. Fletcher, ed., pp. 267-277, 1966.

Bjørgo, E., O.M. Johannessen, and M.W. Miles, Analysis of merged SSMR-SSM/I time series of Arctic and Antarctic sea ice parameters 1978-1995. *Geophys. Res. Lett.*, *24*(4), 413-416, 1997.

Bromwich, D.H., T.R. Parish, and C.A. Zorman, The confluence Zone of the intese katabatic winds at the Terra Nova Bay, Antarctica, as derived from airborne sastrugi surves and mesoscal numerical modeling, J. Geophys. res., 95(D5), 5495-5509, 1990.

Budyko, M.I., Polar ice and climate, In Proceedings of the Symposium of the Arctic Heat Budget and Atmospheric Circulation, ed. by J.O. fletcher (ed), RM5233-NSF, Rand Corporation, Santa Monica, CA, 3-21, 1966.

Businger, S., and R. J. Reed, Polar lows, in Polar and Arctic Lows, Twitchell, P. F., E. A. Rasmussen, and K. L. Davidson, eds., A. Deepak, Hampton, VA, pp. 3-45, 1989.

Carleton, A. M., Satellite climatological aspects of the "polar low" and "instant occlusion," Tellus 37A, 433-450, 1985.

Cavalieri, D. J., NASA Sea Ice Validation Program for the Defense Meteorological Satellite Program Special Sensor Microwave Imager, J. Geophys. Res., 96, 21,969- 21,970, 1991.

Cavalieri, D. J., The validation of geophysical parameters using multisensor data, Chapter 11 in Microwave Remote Sensing of Sea Ice, edited by F. D. Carsey, American Geophysical Union Monograph 68, 233-242, 1992.

Cavalieri, D. J., and S. Martin, The contribution of Alaskan, Siberian, and Canadian coastal polynyas to the cold halocline layer of the Arctic Ocean, *J. Geophys. Res.*, 18,343-18,362, 1994.

Cavalieri, D. J., P. Gloersen, and W. J. Campbell, Determination of sea ice parameters with the Nimbus 7 SMMR, J. Geophys. Res., 89, 5355-5369, 1984.

Cavalieri, D. J., J. Crawford, M. R. Drinkwater, D. Eppler, L. D. Farmer, R. R. Jentz and C. C. Wackerman, Aircraft active and passive microwave validation of sea ice concentration from the DMSP SSM/I, *J. Geophys. Res.*, 96, 21,989-22,008, 1991.

Cavalieri, D.J., C.L. Parkinson, P. Gloersen, J.C. Comiso, and H.J. Zwally, Deriving long-term time series of sea ice cover from satellite passive microwave data sets, *J. Geophys. Res.*, *104*(C7), 15803-15814, 1999.

Cho, K., N. Sasaki, H. Shimoda, T. Sakata, and F. Nishio, Evaluation and improvement of SSM/I sea ice concentration algorithms for the Sea of Okhotsk, *J. Remote Sensing Soc. of Japan, 16*(2), 47-58, 1996.

Comiso, J. C., Sea ice effective microwave emissivities from satellite passive microwave and infrared observations, J. Geophys. Res., 88, 7686-7704, 1983.

Comiso, J. C., Characteristics of winter sea ice from satellite multispectral microwave observations, *J. Geophys. Rev., 91*(C1), 975-994, 1986.

Comiso, J.C., Arctic Multiyear ice Classification and Summer Ice Cover using Passive Microwave Satellite Data, *J. Geophys. Res*., 95, 13411-13422, 1990.

Comiso, J.C., SSM/I Concentrations using the Bootstrap Algorithm, *NASA RP, 1380*, 40pp, 1995.

Comiso, J. C. and K. Steffen, Studies of Antarctic sea ice concentrations from satellite observations and their applications, *J. Geophys. Res., 106*(C12), 2001.

Comiso, J. C. and C. W. Sullivan, Satellite microwave and in-situ observations of the Weddell Sea Ice Cover and its Marginal Ice Zone, *J. Geophys. Res., 91(*C8), 9663-9681, 1986.

Comiso, J.C., and R. Kwok, The summer Arctic sea ice cover from satellite observations, J. *Geophys. Res.*,101(C2), 28397-28416, 1996.

Comiso, J. C., S. F. Ackley, and A. L. Gordon, Antarctic Sea Ice Microwave Signature and their Correlation with In-Situ Ice Observations, J. Geophys. Res. 89(C1):662-672, 1984.

Comiso, J. C., and H. J. Zwally, Antarctic Sea Ice Concentrations Inferred from Nimbus-5 ESMR and LANDSAT imagery, *J. Geophys. Res., 87*(C8), 5836-5844, 1982.

Comiso, J.C., and H.J. Zwally, Temperature Corrected Bootstrap Algorithm, IEEE *IGARSS'97 Digest*, Volume 3, 857-861, 1997.

Comiso, J. C., T. C. Grenfell, D. L. Bell, M. A. Lange,and S. F. Ackley, Passive Microwave In Situ Observations of Winter Weddell Sea Ice, *J. Geophy. Res., 94*, 10891-10905, 1989.

Comiso, J.C., P. Wadhams, W. Krabill, R. Swift, J. Crawford, and W.Tucker, Top/Bottom multisensor remote sensing of Arctic sea ice, J. Geophy. Res., 96(C2), 2693-2711, 1991.

Comiso, J.C, T.C. Grenfell, M. Lange, A. Lohanick, R.Moore, and P. Wadhams, "Microwave remote sensing of the Southern Ocean Ice Cover," Chapter 12, In, *Microwave Remote Sensing of Sea Ice*, (ed. by Frank Carsey), American Geophysical Union, Washington, D.C., 243-259, 1992.

Comiso, J.C., D. Cavalieri, C. Parkinson, and P. Gloersen, Passive microwave algorithms for sea ice concentrations, *Remote Sensing of the Env., 60*(3), 357-384, 1997.

Gloersen P., W. Campbell, D. Cavalieri, J. Comiso, C. Parkinson, H.J. Zwally, Arctic and Antarctic Sea Ice, 1978-1987: Satellite Passive Microwave Observations and Analysis, *NASA Spec. Publ. 511*, 1992.

Gloersen, P. and Barath, F. T., A Scanning Multichannel Microwave Radiometer for Nimbus-G and SeaSat-A, *IEEE Journal of Oceanic Engineering, OE-2*, 172-178, 1977.

Gloersen P., W. J. Campbell, D. J. Cavalieri, J. C. Comiso, C. L. Parkinson, H. J. Zwally, rctic and Antarctic Sea Ice, 1978-1987: Satellite Passive Microwave Observations and Analysis, NASA Spec. Publ. 511, 1992.

Gloersen, P., E. Mollo-Christensen, and P. Hubanks, Observations of Arctic polar lows with the Nimbus 7 Scanning Multichannel Microwave Radiometer, in Polar and Arctic Lows, P. F. Twitchell, E. A. Rasmussen, and K. L. Davidson, eds., A. Deepak, Hampton, Virginia, pp. 359-371, 1989.

Gloersen, P., T. C. Chang, T. T. Wilheit, and W. J. Campbell, Polar sea ice observations by means of microwave radiometry, in Advanced Concepts and Techniques in the Study of Snow and Ice, H. S. Santeford and J. L. Smith, eds., Nat. Acad. Sci, pp.
541-550, 1974.

Gordon, A., Deep Antarctic convection west of Maud Rise, J. *Phys. Oceanography*., 8, 600-612, 1978.

Gordon, A. L., and J. C. Comiso, Polynyas in the Southern Ocean, *Scientific American*, *256*(6), 90-97, 1988.

Grenfell, T.C., J.C. Comiso, M.A. Lange, H. Eicken, and M.R. Wenshahan, Passive microwave observations of the Weddell Sea during austral winter and early spring, J. Geophys, Res., 99(C5), 9995-10,010, 1994.

Grenfell, T. C., A theoretical model of the optical properties of sea ice in the visible and near infrared, *J. Geophys. Res*., 88, 9723-9735, 1983.

Grenfell, T. C., and J. C. Comiso, Multifrequency passive microwave observations of first-year sea ice grown in a tank, IEEE *Trans. Geoscience and Remote Sensing*, GE-24, 826-831, 1986.

Grenfell, T. C., J. C. Comiso, M. A. Lange, H. Eicken, and M. R. Wenshahan, Passive microwave observations of the Weddell Sea during austral winter and early spring, *J. Geophys, Res*., 99(C5), 9995-10010, 1994.

Grenfell, T.C, D.J. Cavalieri, J.C. Comiso, M.R. Drinkwater, R.G. Onstott, I. Rubinstein, K Steffen, I. Rubinstein, D.P. Winebrenner, "Microwave signatures of new and young ice," Chapter 14, *Microwave Remote Sensing of Sea Ice*, (ed. by Frank Carsey), American Geophysical Union, Washington, D.C., 291-301, 1992.

Honda, M., K. Yamazaki, Y. Tachibana, and K. Takeuchi, Influence of Okhhotsk sea-ice extent on atmospheric circulation, *Geophysical Research Letters*, 23, 3595-3598, 1996.

Jacobs, S. and J. C. Comiso, Satellite passive microwave sea ice observations and oceanic processes in the Ross Sea, Antarctica, *J. Geophys. Res., 94*, 18195-18211, 1989. Jacobs, S.S, and J.C. Comiso, A recent sea-ice retreat west of the Antarctic Peninsula,
Geophys. Res. Letter, 20(12), 1171-1174, 1993.

Jacobs, S.S., and J.C. Comiso, A climate anomaly in the Amundsen and Bellingshausen Seas, *J. Climate, 10*(4), 697-709, 1997.Killworth, P. D., Deep convection in the world ocean, Rev. Geophys. and Space Phys. 21, 1-26, 1983.

Johannessen, O.M., E.V. Shalina and M.W. Miles, Satellite evidence for an Arctic sea ice cover in transformation, *Science, 286*, 1937-1939, 1999.

Jones, P.D., M. New, D.E. Parker, S. Martin, and I.G. Rigor, Surface air temperature and its changes over the past150 years, *Rev. Geophys., 37*, 173-199, 1999.

Kwok, R., J.C. Comiso, and G. Cunningham, Seasonal characteristics of the perennial ice cover of the Beaufort Sea, *J. Geophys. Res.,101*(C2), 28417-28439, 1996.

King, J. C. and S. A. Harangozo, Climate change in the western Antarctic Peninsula since 1945: observations and possible causes, Annals of Glac., 27, 571-575, 1998.

Killworth, P. D., Deep convection in the world ocean, Rev. Geophys. and Space Phys. 21, 1-26, 1983.

Markus, T. and D. J. Cavalieri, A revision of the NASA Team sea ice algorithm, *IEEE Transactions on Geoscience and Remote Sensing, 38*(3), 1387-1298, 2000.

Martin, S., K. Steffen, J.C. Comiso, D.J. Cavalieri, M. Drinkwater, B.M. Holt, "Microwave Remote Sensing of Polynyas," Chapter 15, *Microwave Remote Sensing of Sea Ice*, (ed. by Frank Carsey), American Geophysical Union, Washington, D.C., 303-311, 1992.

Massom, R., *Satellite remote sensing of polar regions*, Lewis Publishers, Florida, 307pp, 1991.

Massom, R.A., J.C. Comiso, A.P. Worby, V. Lytle, and L. Stock, Satellite and in situ observations of regional classes of sea ice cover in the East Antarctic pack in winter, Remote Sensing of the Env., 68(1), 61-76, 1999.

Mätzler, C., R.O. Ramseier, and E. Svendsen, Polarization effects in sea ice signatures, *IEEE J. Oceanic Eng. OE-9*, 33-338, 1984.

Maykut, G. A., Energy exchange over young ice in the central Arctic, J. Geophys. Res., 83(C7), 3646-3658, 1978.

Oelke, C., Atmospheric signatures in sea-ice concentration estimates from passive microwaves: modelled and observed, *Int. J. Remote Sensing, 18*, 1113-1136, 1997.

Parkinson, C. L., J. C. Comiso, H. J. Zwally, D. J. Cavalieri, P. Gloersen, and W. J. Campbell (1987), Arctic Sea Ice 1973- 1976 from Satellite Passive Microwave Observations, NASA Spec. Publ. 489, pp.296, 1987.

Parkinson, C. L., D. J. Cavalieri, P. Gloersen, H. J. Zwally, and J. C. Comiso, Variability of the Arctic Sea Ice Cover 1978-1996, *J. Geophys. Res*., 104, 20,837-20,856, 1999.

Preller, R. H., J. E. Walsh, and J. A. Maslanik, The use of satellite observations in ice cover simulations, Chapter 22, in Microwave Remoate Sensing of Sea Ice, F. D. Carsey (ed.), Geophysical Monograph 68, American Geophysical Union, Washington, DC, 1992.

Rothrock, D. A., Y. Yu, and G. A. Maykut, Thinning of the Arctic sea-ice cover, G*eophys. Res. Lett.*, 26(23), 3469-3472, 1999.

Schluessel, P. and H. Grassl, SST in polynyas: A case study, International Journal of Remote Sensing, 11(6), pp.933-945, 1990.

Steffen, K. and A. Schweiger, NASA team algorithm for sea ice concentration retrieval from the Defense Meteo-rological Satellite Program Special SensorMicrowave Imager: Comparison with Landsat Imagery, J. Geophys. Res., 96(12), 21971-21987, 1991.

Stommel, H., On the smallness of sinking regions in the ocean, Proc. Nat. Acad. Sc., USA 48, 766-772, 1962.

Svendsen, E., K. Kloster, K., B. Farrelly, O. M. Johannessen, J. A. Johannessen, W. J. Campbell, P. Gloersen, D. J. Cavalieri, and C. Matzler, Norwegian Remote Sensing Experiment: Evaluation of the Nimbus 7 Scanning multichannel microwave radiometer for sea ice research, J. Geophys. Res., 88, 2781-2792, 1983.

Swift, C. T., L. S. Fedor, and R. O. Ramseier, An algorithm to measure sea ice concentration with microwave ra-diometers, J. Geophys. Res., 90, 1087-1099, 1985.

Tjuata, S., A.K. Fung, and J.C. Comiso, Effects of Snow Cover on Sea Ice Emission, *IEEE IGARSS'95 Digest*, Vol. 1, 697-699, 1995.

Tjuata, S., A.K. Fung, and M. Dawson, An analysis of scattering and emission from sea ice, *Remote Sensing Review*, *7*, 83-106, 1993.

Vowinckel, E., and S. Orvig, The climate in the north polar basin, in Climate of the Polar Regions, Vol.14 of World Survey of Climatology, Elsevier, Amsterdam, pp. 129-252, 1970.

Tucker III, W.B., D.K. Perovich, A.J. Gow, W.F. Weeks, and M.R. Drinkwater, Physical properties of sea ice relevant to remote sensing, Chapter 2, *Microwave Remote Sensing of Sea Ice*, (ed. by Frank Carsey), American Geophys. Union, Washington, DC., 201-231, 1992.

Wadhams, P., and N. Davis, Further evidence of ice thinning in the Arctic Ocean, *Geophy. Res. Lett.*, *27*(24), 3973-3976, 2000.

Walsh, J. E., and H. J. Zwally, Multiyear sea ice in the Arctic: model- and satellite-derived, J. Geophys. Res. 95, 11,613-11,628, 1990.

Wensnahan, M., Maykut, G. A., Grenfell, T. C., and D. P. Winebrenner, Passive microwave remote sensing of thin sea ice using principal component analysis, J. Geophys. Res., 98, 12,453-12,468, 1993.

Worby, A. P., and R. A. Massom, The structure and properties of sea ice and snow cover in East Antarctic pack ice, Antarctic CRC, Research report, 7, 191 pp., 1995. Worby, A.P., and J. Comiso, A study of the Antarctic Sea Ice Edge using SSM/I-Derived and in situ Observations, *IGARSS Digest 2001*, Sydney, Australia, July 2001.

Worby, A.P., and R.A. Massom, The structure and properties of sea ice and snow cover in East Antarctic pack ice, *Antarct. CRC Res. Rep., 7,* 191 pp., Antarct. Coop. Res. Cent., Hobart, Tasmania, 1995.

Yamanouchi, T., and K. Seko, Antarctica from NOAA satellites, National Institute of Polar Research Press, Tokyo, Japan, 91 pp., 1992.

Zwally, H. J., J. C. Comiso, C. L. Parkinson, W. J. Campbell, F. D. Carsey, and P. Gloersen, Antarctic Sea Ice 1973-1976 from Satellite Passive Microwave Observations, *NASA Spec. Publ. 459*, 1983.

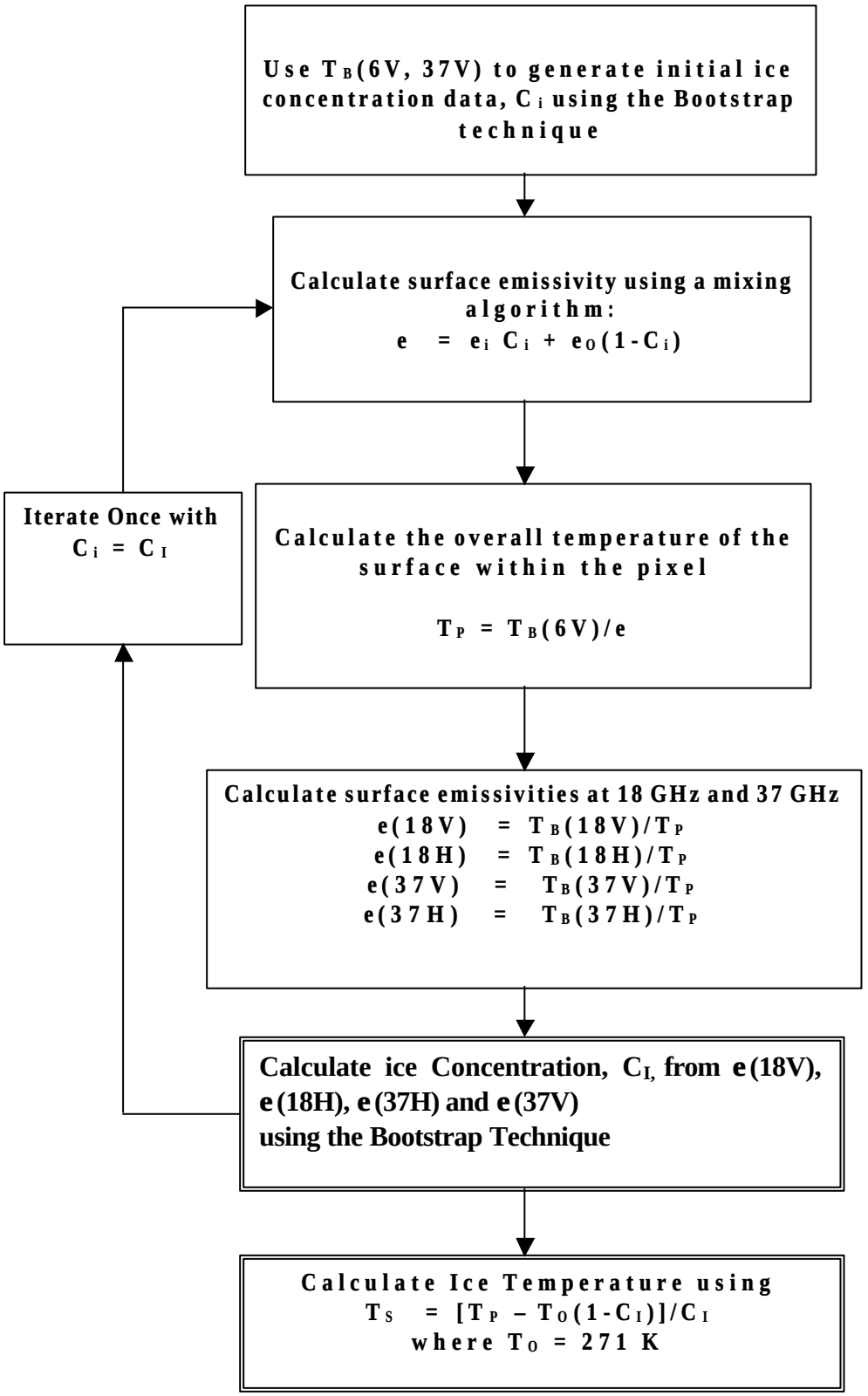

Figure 3. Schematics of the AMSR Bootstrap Algorithm

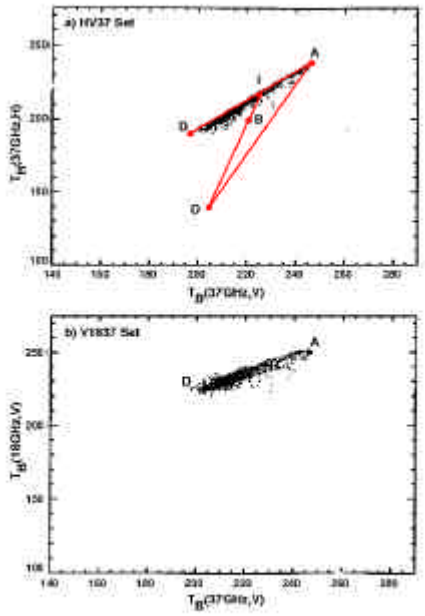
a) H/37 Set
A
B
C
D
T_B(37GHz,H)
T_B(37GHz,V)
b) V1837 Set
A
D
T_B(18GHz,V)
T_B(37GHz,V)

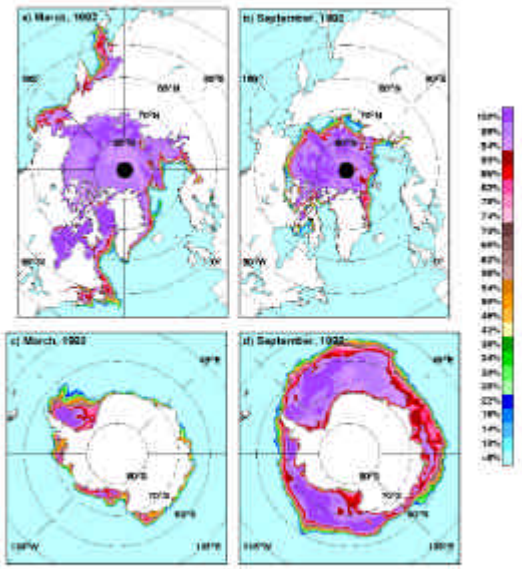
a) March, 1992
b) September, 1992
c) March, 1992
d) September, 1992

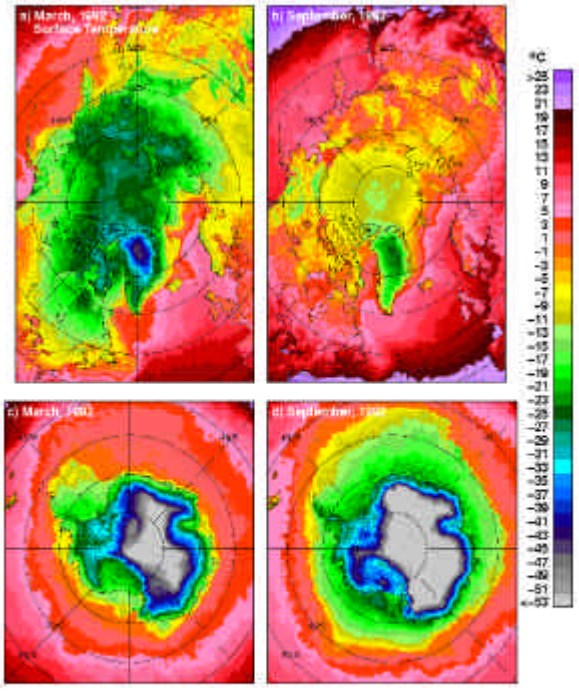
a) March, 1992
Surface Temperature
b) September, 1992
c) March, 1992
d) September, 1992
°C

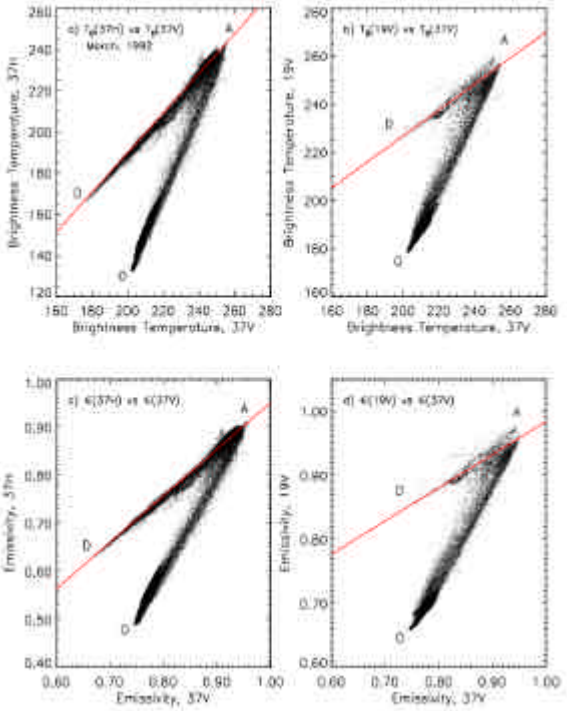
a) T_B(37H) vs T_B(37V)
March, 1992
b) T_B(19V) vs T_B(37V)
A
B
C
D
Brightness Temperature, 37H
Brightness Temperature, 19V
Brightness Temperature, 37V
c) ε(37H) vs ε(37V)
d) ε(19V) vs ε(37V)
Emissivity, 37H
Emissivity, 19V
Emissivity, 37V

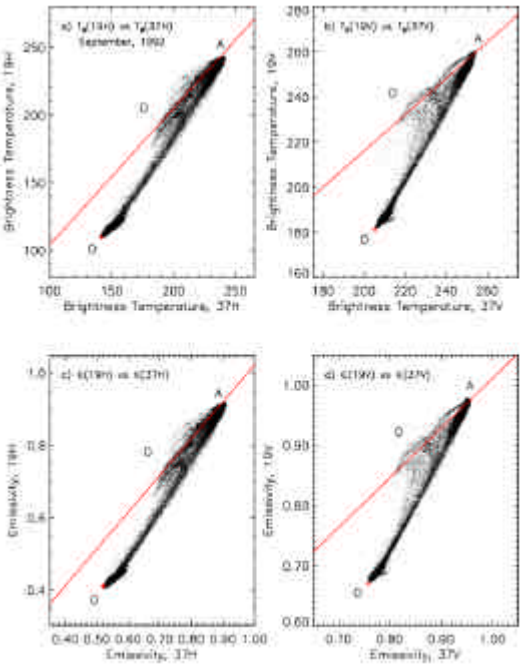
a) T_B(19H) vs T_B(37H)
September, 1992
b) T_B(19V) vs T_B(37V)
c) ε(19H) vs ε(37H)
d) ε(19V) vs ε(37V)
A
D
Brightness Temperature, 19H
Brightness Temperature, 37H
Brightness Temperature, 19V
Brightness Temperature, 37V
Emissivity, 19H
Emissivity, 37H
Emissivity, 19V
Emissivity, 37V

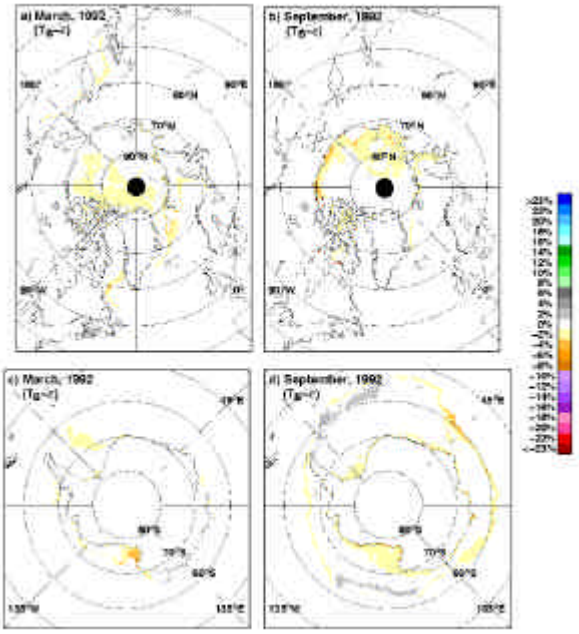
a) March, 1992
(Tg-c)
b) September, 1992
(Tg-c)
c) March, 1992
(Tg-c)
d) September, 1992
(Tg-c)

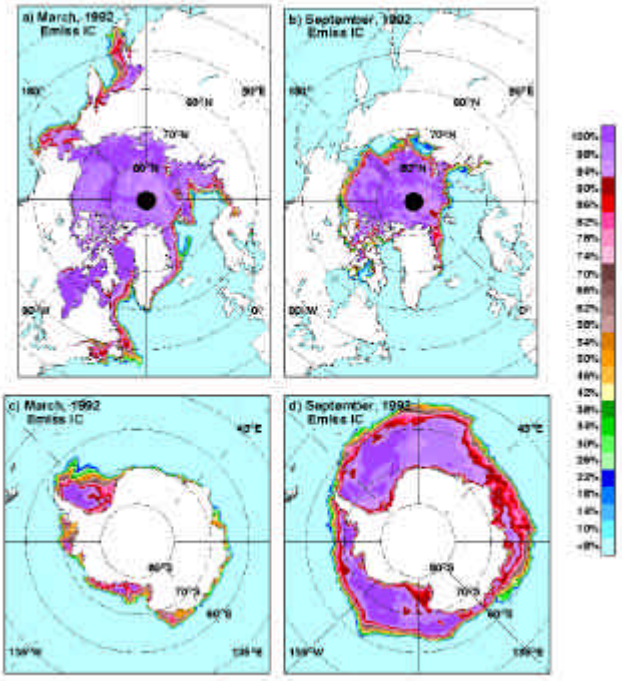
a) March, 1992
Emiss IC
b) September, 1992
Emiss IC
c) March, 1992
Emiss IC
d) September, 1992
Emiss IC

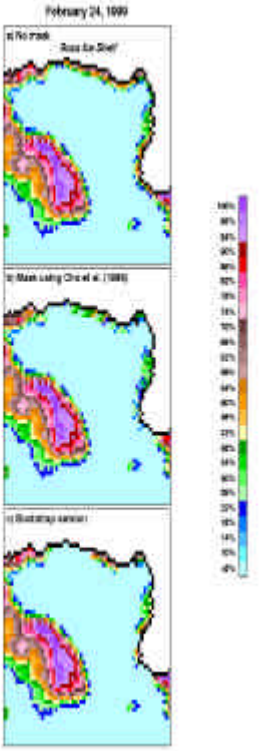
February 24, 1999
a) No mask
Ross Ice Shelf
b) Mask using Chen et al. (1995)
c) Bootstrap version

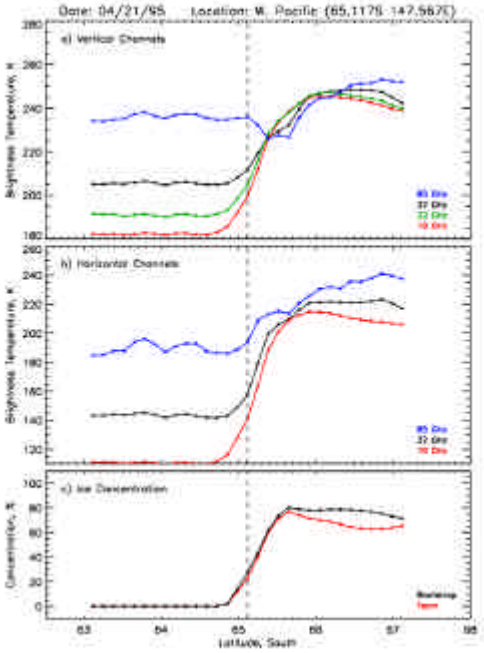
Date: 04/21/95 Location: W. Pacific (65.11°S 147.56°E)
a) Vertical Channels
b) Horizontal Channels
c) Ice Concentration
Brightness Temperature, K
Concentration, %
Latitude, South

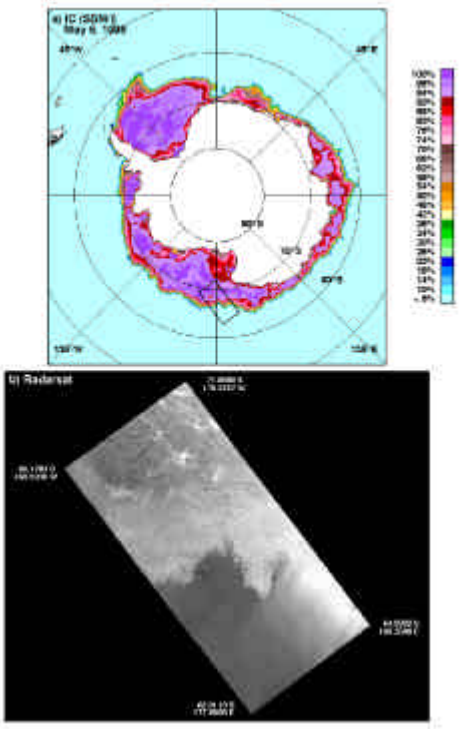
a) IC (SSM/I)
b) Radarsat

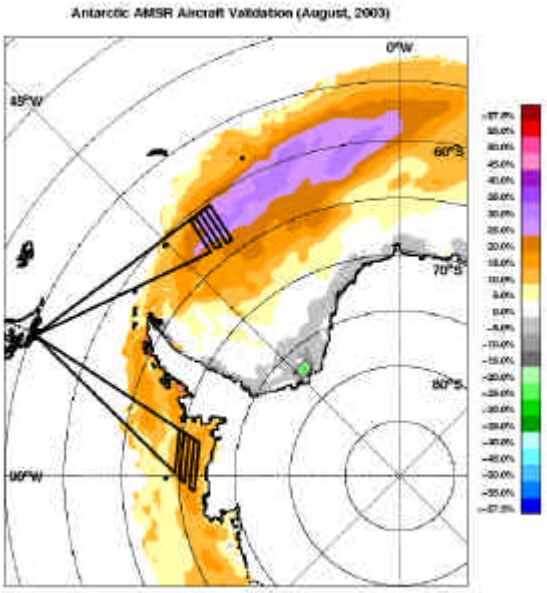
Antarctic AMSR Aircraft Validation (August, 2003)
0°W
45°W
90°W
60°S
70°S
80°S

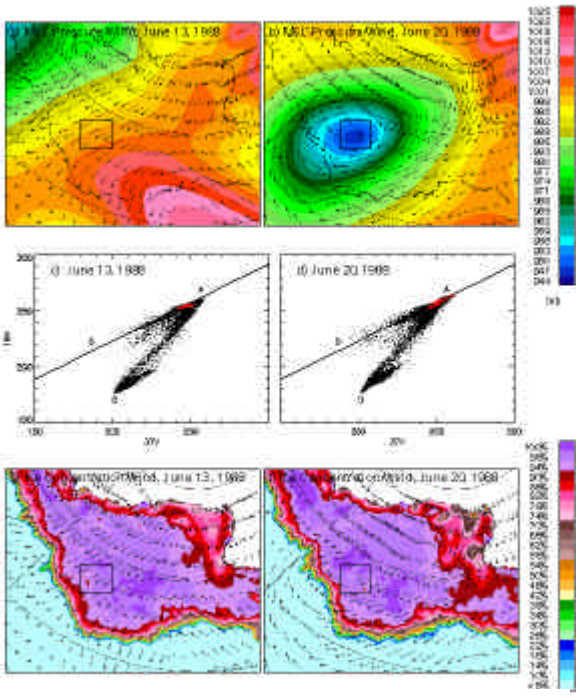
c) June 13, 1988
d) June 20, 1988